CHEMISTRY OF MATERIALS

Article

pubs.acs.org/cm

Shape Control of Ag Shell Growth on Au Nanodisks

Soonchang Hong,[†] Yoonjung Choi,[†] and Sungho Park*[,†,‡]

[†]Department of Chemistry, [‡]Department of Energy Science and SKKU Advanced Institute of Nanotechnology, Sungkyunkwan University, Suwon 440-746, South Korea

Supporting Information

ABSTRACT: Core−shell (Au@Ag) bimetallic nanoparticles containing a Au nanodisk in the core were synthesized using Au nanodisks as seeds. The growth direction of the Ag shell on the gold nanodisks could be tuned by the presence of iodide ions. Without the I^- ions, the Ag shell was formed homogeneously over the entire surface of the flat Au nanodisks, while the presence of I^- induced the selective coating of the Ag shell in the direction perpendicular to the basal plane of the nanodisks. The resulting core−shell (Au@Ag) bimetallic nanoparticles could be further converted to hollow nanostructures containing a central Au nanodisk via galvanic replacement reactions.

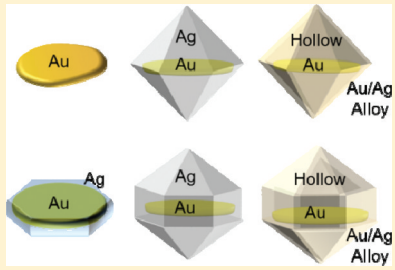

KEYWORDS: *Au nanodisk, bimetallic nanoparticles, core−shell nanoparticles, surface plasmon, galvanic replacement*

Bimetallic core−shell nanoparticles have received considerable attention due to their tunable and unique optical, magnetic, electronic, and catalytic properties because of the synergy effect or independent properties of two different components. Among them, noble metal nanostructures, especially gold and silver core−shell,[1−9] and alloy[16−19] nanocrystals have attracted increased attention because of their simple synthetic methods and easy shape control. Many studies have demonstrated the synthetic routes to various shapes of Au@Ag core−shell nanostructures including spheres,[1,5] rods,[2,9] and plates.[6,8] It is rarely found, however, the synthetic route to control the shapes of both core and shell simultaneously. The shape control of shell on nanocrystals is difficult because the shell component is reduced and grows on the core surface directly. Usually, the shell shape resembles an exterior core shape. It motivated us to develop new methods for synthesizing nanocrystals with different core and shell shapes in a controlled fashion.

In this study, we synthesized Au@Ag nanostructures containing a central Au nanodisk that was used as a seed. We selectively controlled the Ag shell growth direction by introducing iodide ions (I^-) during the synthesis. Without the I^- ions, the Ag shell was formed homogeneously over the entire surface of the Au nanodisk, leading to the formation of hexagonal nanoplates. In the presence of I^-, however, dodecahedral nanostructures were generated perpendicular to the basal plane of the Au nanodisk. The resulting Au@Ag nanostructure could be further converted to hollow structures via galvanic replacement between Ag and Au ions. The homogeneity and narrow size distribution of the resulting samples allowed the characterization of their each corresponding optical property by UV−vis-NIR spectroscopy.

EXPERIMENTAL SECTION

Materials. $HAuCl_4 \bullet 3H_2O$ was purchased from KOJIMA. Sodium citrate (99%) was purchased from YAKURI. Sodium borohydride (98%) and silver nitrate were purchased from JUNSEI. Sodium iodide (NaI) and ascorbic acid were purchased from Sigma Aldrich. Sodium hydroxide (NaOH) was purchased from SAMCHUN, and cetyltrimethyl ammonium bromide (CTAB) was supplied by Fluka. All involved reagents were dissolved in distilled water (18.2 MΩ) that was prepared by a Milli-Q water purification system.

Synthesis of Triangular Nanoplates. Triangular nanoplates were prepared from 5 nm sphere seed by a three-step seed mediated method with iodide ions which was reported previously.[10] Briefly, 0.5 mL of a 20 mM aqueous $HAuCl_4 \cdot 3H_2O$ solution and 1 mL of a 10 mM aqueous solution of sodium citrate and 1 mL of a 100 mM aqueous $NaBH_4$ (Ice-cold) solution were added to 36.5 mL of deionized water with vigorous stirring.

In order to prepare triangular nanoplates, three labeled flasks were prepared. A mixture of 108 mL of 0.05 M aqueous CTAB solution and 54 μL of 0.1 M aqueous NaI solution was divided into three containers labeled with 1, 2, and 3. Nine mL of mixture was added in each container 1 and 2. The remaining mixture (90 mL) was added in container 3. Then, a mixture of 125 μL of a 20 mM aqueous $HAuCl_4 \cdot 3H_2O$ solution, 50 μL of 100 mM NaOH, and 50 μL of 100 mM ascorbic acid was added to each container 1 and 2. A mixture of 1.25 mL of 20 mM $HAuCl_4 \cdot 3H_2O$, 0.5 mL of 100 mM NaOH, and 0.5 mL of 100 mM ascorbic acid was added to container 3.

One mL of the seed solution was added to container 1 with mild shaking, followed by adding 1 mL of container 1 solution into container 2. After gentle shaking, the whole solution of container 2 was added to container 3.

Synthesis of Au@Ag Nanoparticles. After a purifying step,[12] 1 mL of a 20 mM aqueous $HAuCl_4 \cdot 3H_2O$ solution was added in 20 mL of triangular nanoplates. Triangular nanoplates were etched by gold ions. As a result, triangular nanoplates transform to gold nanodisks, and then residual gold ions were removed from centrifugation (5000 rpm × 5 min). Three mL of 0.05 M CTAB, 2 mL of redispersed gold nanodisks, 75 μL of 100 mM NaOH, and 500 μL of 10 mM ascorbic acid were added in the round-bottom flask (in the presence or absence

Received: July 28, 2011
Revised: November 14, 2011
Published: November 17, 2011

of iodide ions (50 μM)). In the absence of iodide ions, 500 μL of a 1 mM aqueous $AgNO_3$ solution was added into the mixtures. On the other hand, 600 and 1000 μL of a 1 mM aqueous $AgNO_3$ solution were added into the mixtures with 50 μM iodide ions to synthesize dodecahedron and elongated polyhedron, respectively.

For galvanic replacement reaction, 100 μL of a 20 mM aqueous $HAuCl_4$ solution was added in 10 mL of a 0.05 M CTAB solution. A total of 3 mL of the prepared $HAuCl_4$ solution was added in 4 mL of dodecahedron or elongated polyhedron. These solutions were kept for about 3 hours at room temperature with vigorous stirring.

Characterization. A JEM-2100F was used to acquire transmission electron microscopy (TEM) images. Scanning electron microscopy (SEM) images were obtained by using JEOL 7000F and JEOL 7600F. UV−vis absorption spectra were taken by using an S-3100 spectrophotometer (Scinco).

RESULTS AND DISCUSSION

Figure 1 shows a schematic diagram of the steps involved in the dissolution process of Au triangular nanoplates, selective

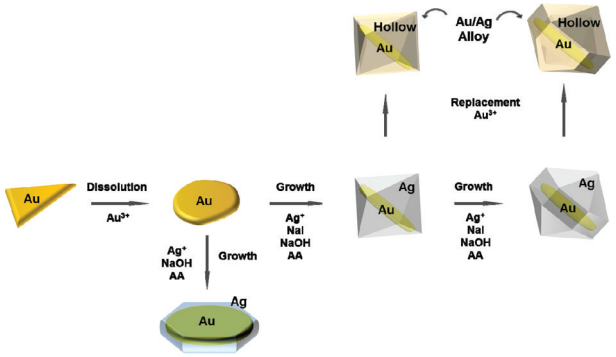

Figure 1. Schematic diagram of formation of core@shell Au@Ag nanostructures and hollow structures. AA is ascorbic acid.

growth of the Ag shell, and galvanic replacement between Ag and Au ions, which systematically lead to various types of nanostructures. First, Au nanodisks were synthesized by selectively dissolving the vertices of Au triangular nanoplates (Figure 2) that had been prepared according to a previously

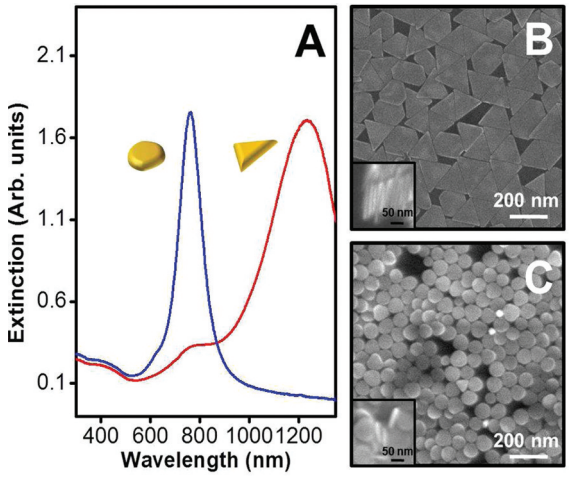

Figure 2. Vis-near IR spectra (A) and SEM images (B, C) of Au triangular nanoplates and nanodisks. Left lower insets show their corresponding side-view. The edge length of the triangular nanoplate is 150 (±19) nm, and the thickness is 12 (±2) nm. The diameter of the Au nanodisk is 74 (±4) nm, and the thickness is 10 (±2) nm.

published three-step, seed-mediated method.[10−12] The average edge length of the triangular nanoplates was 150 (±19) nm, and the average thickness was 12 (±2) nm. The addition of Au^{3+} ions into the solution containing Au triangular nanoplates led to the formation of Au nanodisks because the sharp tips of the triangular plates were selectively etched due to the lower standard redox potential at the vertices.[13,14] The nanoplates shape transformation steps have been monitored with time-resolved UV−vis-NIR spectroscopy in more detail (Figure S1). In the etching process, the spectra clearly reveal two distinct changes, the one of which is the peak shift at 1230 nm to shorter wavelength (at 764 nm after 30 min) as the tips of triangular nanoplates become rounded. This band is assigned to the in-plane dipole resonance associated with the Au nanoplates. Concurrently, the peak intensity at 395 nm, which is the feature of $AuCl_4^-$ ions, becomes weak as a result of $AuCl_4^-$ reduction. The reduction of $AuCl_4^-$ ions occurs because of the presence of reducing agent (ascorbic acid) and the oxidation of $Au_{vertex}(s)$ of triangular nanoplates. The average diameter of the Au nanodisks was 74 (±4) nm, and the average thickness was 10 (±2) nm.

Figure 3 shows TEM images, SEM images and EDS line profile of the Au@Ag nanostructures. Dodecahedron and

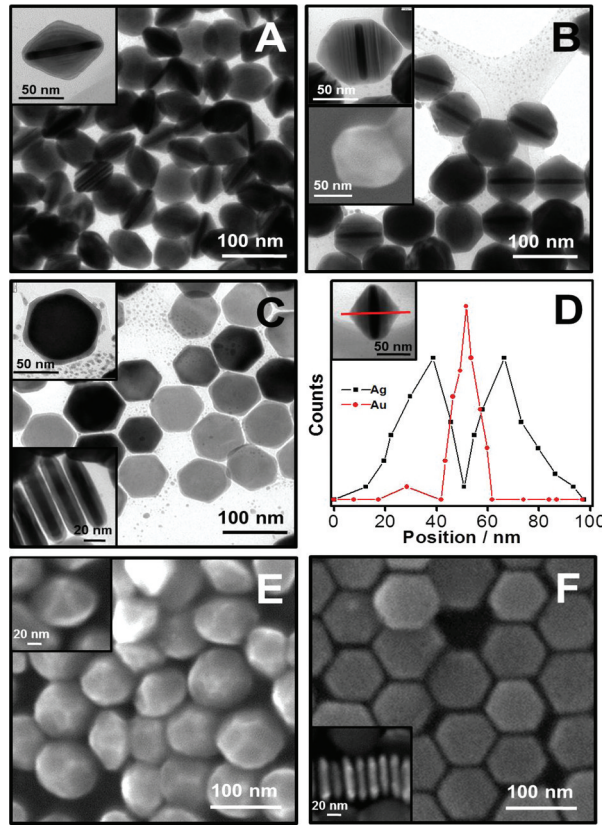

Figure 3. TEM images (A, B, C) and SEM images (E, F) of Au@Ag nanocrystals in the presence of iodide ions (A, B, E) and in the absence of iodide ions (C, F). Each left upper inset shows a zoom-in image for each sample. The left-lower inset in (B) represents the SEM image. The added amount of 1 mM $AgNO_3$ is 600, 1000, and 500 μL for (A), (B), and (C), respectively. The left lower inset in (C, F) shows the side view of stacked nanoplates. (D) EDS line profile for Au@Ag nanocrystals containing gold nanodisk in the core.

elongated polycahedron Au@Ag nanoparticles were synthesized using different amounts of silver (600 μL and 1000 μL of

dx.doi.org/10.1021/cm2021966 | Chem. Mater. 2011, 23, 5375−5378

1 mM $AgNO_3$) in the presence of I^- ions (Figure 3A and B), while hexagonal Au@Ag nanoplates were synthesized in the absence of I^- ions (Figure 3C). All nanoparticles contained gold nanodisks in the core, which are clearly distinguishable in the TEM images by their contrast. In the presence of I^- ions, the Ag shell grew perpendicular to the basal plane of the Au nanodisks with no noticeable XY-directional growth (Figure 3A). Initially, the shape of the Au@Ag nanostructure was a dodecahedron. Further growth of the Ag shell occurred on the sides of the Au nanodisks, leading to the elongated polyhedrons (Figure 3B). As clearly indicated in the magnified image in the upper left inset, the thickness of the middle part was elongated compared to those of the dodecahedrons shown in Figure 3A. All of the nanoparticles had a flat Au nanodisk at the core, which indicates that the Ag shell growth occurred under the given experimental conditions exclusively on the Au surface without a new nucleation process. Without I^- ions, the Ag shell grew homogeneously over the entire surface of the gold nanodisk (Figure 3C). Interestingly, Ag reduction on the side of the round-shaped Au nanodisks led to the formation of hexagonal nanoplates with a well-defined tip morphology during the Ag ripening process. The energy dispersive spectroscopy (EDS) line profile of the Au@Ag nanoparticles indicates that silver fully covered the gold nanodisks (Figure 3D). In the center of the nanocrystal, gold was detected at a high peak intensity compared to the low intensity of silver. An intense silver peak was observed on the edge of the particle, while there was no noticeable signal for Au. In order to investigate the surface structure in more detail, we took field emission scanning electron microscopy (FESEM) images for dodecahedron and hexagonal Au@Ag nanoplates, as shown in Figure 3, parts E and F, respectively. The magnified image in the upper left inset of Figure 3E shows that the resulting Au@Ag nanocrystal has 12 facets, with six on each face of the nanodisk. Although the gold nanodisk seeds appeared to have round shapes, they were actually hexagonal nanoplates with dull vertexes. When Ag ions were deposited on the planes of the Au nanodisks, the Au@Ag nanocrystals initially evolved to a dodecahedral structure. When this process proceeded further, the Au@Ag nanocrystals retained the dodecahedral structure but instead additional faces appeared in the middle part. However, when I^- ions are absent, hexagonal nanoplates were synthesized at a high yield with a homogeneous thickness (Figure 3F, and the left lower inset).

UV–visible-near IR spectrum of each sample shows their characteristic surface plasmon resonance bands, which is also noticeable by its distinct color, as displayed the inset photograph (Figure 4A). Hexagonal Au@Ag nanoparticles showed their localized surface plasmon resonance peak maximum at 637 nm (blue line, in panel A), whereas the dodecahedrons showed their peak maximum at 517 nm (red line), and the elongated polyhedrons were at 505 nm (green line). When $AgNO_3$ and ascorbic acid were added into the Au nanodisk solution in the presence of I^- ions, we can observe that the in-plane dipole mode gradually blue shifts because the thickness of nanodisks increased and the edges became more rounded as Ag^+ ions were reduced at Au nanodisk surface (Figure 4B). As Ag^+ ions were reduced and Au@Ag nanocrystals were formed, a characteristic peak of silver about at 400 nm appeared and red shifts. The peak intensity increased as the ratio of silver on Au@Ag nanocrystals increased during the growth reaction.

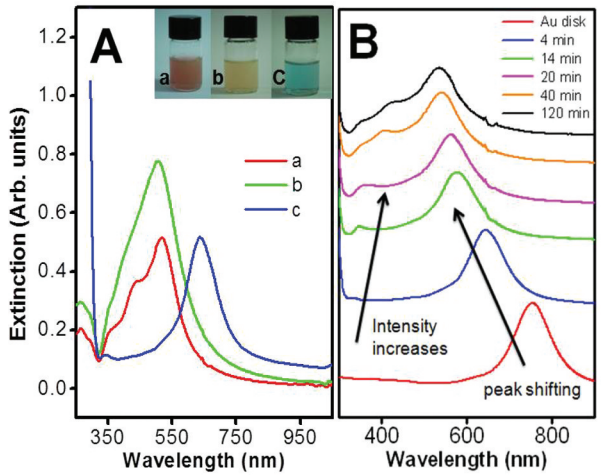

Figure 4. (A) UV–visible-near IR extinction spectra for Au@Ag nanoparticles corresponding to the TEM image in Figure 3 (samples (A), (B), and (C) are represented by (a), (b), and (c), respectively). The corresponding photograph image is represented in the right upper inset. (B) Time-resolved UV–vis-near IR spectra of the growth process of nanodisks to Au@Ag nanocrystals after adding $AgNO_3$ and ascorbic acid to the nanodisk solution.

The detailed crystal structures were investigated using high-resolution transmission electron microscopy (HRTEM) and selected area electron diffraction (SAED) patterns (Figure 5).

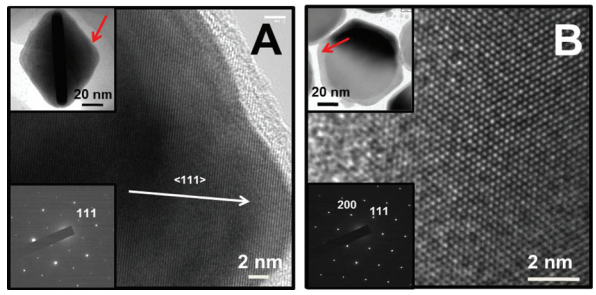

Figure 5. HRTEM images of Au@Ag nanocrystals, (A) dodecahedrons and (B) hexagonal nanoplates. The left upper images show their whole shape, and the red arrow indicates the zoom-in points. The left lower insets show electron diffraction patterns through the red-arrow indicated region.

The SAED pattern and fringe spacing (0.24 nm) indicate that silver grew along the {111} direction in the presence of I^- ions. On the other hand, in the absence of I^- ions, the top surfaces of the hexagonal shaped nanoparticles were {110} facets (Figure 5B).

We suggest the formation mechanism of Au@Ag nanocrystals based on the HRTEM images and results from previously published studies. In previously reported experiments, the growth of Ag shells on Au seeds was controlled using PVP as a blocking agent at specific facets.[7,9] In our experiment, instead of PVP, iodide ions played a key role in blocking specific facets of the Au nanodisks. The Ag^+ ions formed AgBr, which then bound to the surfaces of the Au nanodisks. Br^- ions were present in the nanodisk solution because CTAB was used as a surfactant. When I^- ions were present in the solution, AgI was formed because Ag^+ ions have a higher affinity for iodide ions than they do for bromide ions ($K_{sp}(AgBr) = 5.0 \times 10^{-13}$, $K_{sp}(AgI) = 8.3 \times 10^{-17}$).[15]

dx.doi.org/10.1021/cm2021966 | Chem. Mater. 2011, 23, 5375–5378

The top surfaces of the Au nanodisks had {111} crystallinities, and it has been reported that iodide ions effectively block {111} facets and prevent the growth of Au nanocrystals.[10] Therefore, we believe that the I^- ions bound to the Au {111} facets also bound Ag^+ ions to form AgI on the Au surface. The anchored Ag^+ ions were subsequently reduced to Ag by the reducing agent (ascorbic acid) in the growth solution, leading to Ag shell growth in the direction of the {111} facets. On the contrary, when there are no I^- ions, Ag grew over the surfaces of the Au nanodisks without selectivity.

The resulting Au@Ag nanostructures could be further converted into hollow structures via galvanic replacement reactions (Figure 6).[20−23] When gold ions were added into the

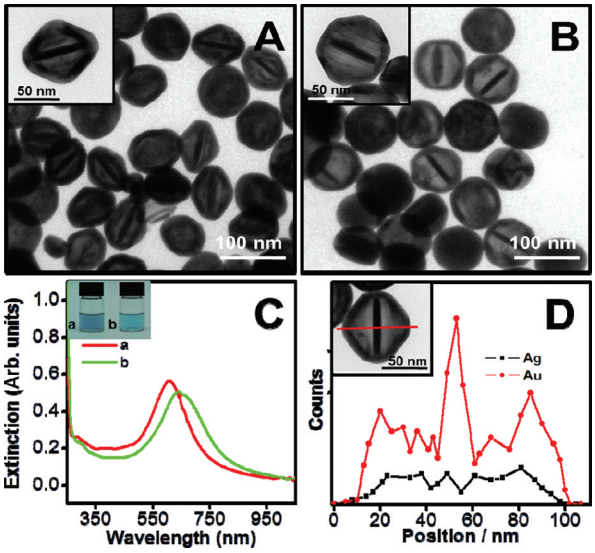

Figure 6. TEM images show the products after the galvanic replacement with Au ions, (A) dodecahedron, and (B) elongated polyhedron. (C) UV−vis-NIR spectra of products (A) and (B) corresponding to (a) and (b). The inset shows their photographic image. (D) Line-mapping of dodecahedron.

Au@Ag nanocrystals, Ag was oxidized to Ag^+, and $AuCl_4^-$ was reduced to Au because of the difference in the reduction potentials between Ag^+/Ag (0.8 V vs SHE) and $AuCl_4^-/Au$ (0.99 V vs SHE).[7] The Au@Ag nanoparticles (dodecahedrons and elongated polyhedrons) were converted into hollow structures, retaining their original shapes through the galvanic replacement reaction and the Kirkendall effect (Figure 6A, B). The central gold nanodisks maintained their structures without distortion after the galvanic replacement reaction.

When the Ag shells were replaced with Au, the peak positions of the dodecahedrons and elongated polyhedrons appeared at 648 and 607 nm, respectively (Figure 6C). Compared to their original peak positions (Figure 4A), these peaks were far red-shifted. The color of each nanoparticle solution showed a change from pink (dodecahedron) and yellow (elongated polyhedron) to cyan (hollow nanostructures). The EDS line profile analysis showed that there was a trace amount of Ag in the matrix of Au, reflecting the presence of Au/Ag alloy nanoshells (Figure 6D).

CONCLUSION

We synthesized unusual dodecahedron and elongated polyhedron Au@Ag nanostructures from Au triangular nanoplates. The resulting nanoparticles could be converted into hollow nanostructures with central Au nanodisks via galvanic replacement. By controlling the amounts of Ag^+ and I^- ions in the solution, we could control the Au@Ag nanostructures. It is especially important to understand the roles of iodide ions in order to fine-tune the nanostructure. Using the TEM images and EDS line-mappings, we confirmed that the products were composed of central Au nanodisks and outer Ag shells depending on the synthetic conditions.

ASSOCIATED CONTENT

Supporting Information

Figure S1. This material is available free of charge via the Internet at http://pubs.acs.org.

AUTHOR INFORMATION

Corresponding Author

*E-mail: spark72@skku.edu.

ACKNOWLEDGMENTS

This work was supported by the National Research Foundation of Korea (2011-0027911, 2011-0003385, World Class University (WCU): R31-2008-10029, and Priority Research Centers Program: NRF-20100029699).

REFERENCES

(1) Freeman, R. G.; Hommer, M. B.; Grabar, K. C.; Jackson, M. A.; Natan, M. J. *J. Phys. Chem.* **1996**, *100*, 718.
(2) Liu, M.; Guyou-Sionnest, P. *J. Phys. Chem. B* **2004**, *108*, 5882.
(3) Xue, C.; Millstone, J. E.; Li, S.; Mirkin, C. A. *Angew. Chem.* **2007**, *119*, 8588.
(4) Seo, D.; Yoo, C. I.; Jung, J.; Song, H. *J. Am. Chem. Soc.* **2008**, *130*, 2940.
(5) Olson, T. Y.; Schwartzberg, A. M.; Orme, C. A.; Talley, C. E.; O'Connell, B.; Zhang, J. Z. *J. Phys. Chem. C* **2008**, *112*, 6319.
(6) Tsuji, M.; Matuso, R.; Jiang, P.; Miyamae, N.; Ueyama, D.; Nishio, M.; Hikino, S.; Kumagae, H.; Kamarudin, K. S. N.; Tang, X.-L. *Cryst. Growth Des.* **2008**, *8*, 2528.
(7) Seo, D.; Song, H. *J. Am. Chem. Soc.* **2009**, *131*, 18210.
(8) Yoo, H.; Millstone, J. E.; Li, S.; Jang, J.-W.; Wei, W.; Wu, J.; Schatz, G. C.; Mirkin, C. A. *Nano Lett.* **2009**, *9*, 3038.
(9) Cho, E. C.; Camargo, P. H. C.; Xia, Y. *Adv. Mater.* **2010**, *22*, 744.
(10) Millstone, J. E.; Wei, W.; Jones, M. R.; Yoo, H.; Mirkin, C. A. *Nano Lett.* **2008**, *8*, 2526.
(11) Millstone, J. E.; Park, S.; Shuford, K. L.; Qin, L.; Schatz, G. C.; Mirkin, C. A. *J. Am. Chem. Soc.* **2005**, *127*, 5312.
(12) Ha, T. W.; Kim, Y. J.; Park, S. H. *Chem. Commum.* **2010**, *46*, 3164.
(13) Hong, S.; Shuford, K. L.; Park, S. *Chem. Mater.* **2011**, *23*, 2011.
(14) Rodriguez-Fernandez, J.; Perez-Juste, J.; Mulvaney, P.; Liz-Marzan, L. M. *J. Phys. Chem. B* **2005**, *109*, 14257.
(15) Harris, D. C. *Quantitative Chemical Analysis*; Freeman W. H. and Company: New York, 2003.
(16) Link, S.; Wang, Z. L.; El-sayed, M. A. *J. Phys. Chem. B* **1990**, *103*, 3529.
(17) Henkel, A.; Jakab, A.; Brunklaus, G.; Sonnichsen, C. *J. Phys. Chem. C* **2009**, *113*, 2200.
(18) Wang, C.; Peng, S.; Chan, R.; Sun, S. *Small* **2009**, *5*, 567.
(19) He, W.; Wu, X.; Liu, J.; Zhang, K.; Chu, W.; Feng, L.; Hu, X.; Zhou, W.; Xie, S. *Langmiur* **2010**, *26*, 4443.
(20) Metraux, G. S.; Cao, Y. C.; Jin, R.; Mirkin, C. A. *Nano Lett.* **2003**, *3*, 519.
(21) Lu, X.; Tuan, H.-Y.; Chen, J.; Li, Z.-Y.; Korgel, B. A.; Xia, Y. *J. Am. Chem. Soc.* **2007**, *129*, 1733.
(22) Sun, Y.; Mayers, B.; Xia, Y. *Adv. Mater.* **2003**, *15*, 641.
(23) Liu, L.; Yoo, S.-H.; Park, S. *Chem. Mater.* **2010**, *22*, 2681.